Published in final edited form as:
Magn Reson Med. 2010 March ; 63(3): 625–632. doi:10.1002/mrm.22242.

A Concentration-Independent Method to Measure Exchange Rates in PARACEST Agents

W. ThomasDixon[1], **Jimin Ren**[2], **Angelo J. M. Lubag**[2], **James Ratnakar**[2], **Elena Vinogradov**[3], **Ileana Hancu**[1], **Robert E. Lenkinski**[3], and **A. Dean Sherry**[2,4]

[1] GE Global Research, Bldg. nmr-132, One Research Circle, Niskayuna, NY 12309

[2] Advanced Imaging Research Center, Department of Radiology, 5323 Harry Hines Blvd., University of Texas Southwestern Medical Center, Dallas, TX75390

[3] Department of Radiology, Beth Israel Deaconess Medical Center, 330 Brookline Ave., Boston, MA 02215

[4] Department of Chemistry, University of Texas at Dallas, Richardson, TX75083

Abstract

The efficiency of chemical exchange saturation transfer agents is largely determined by their water or proton exchange kinetics yet methods to measure such exchange rates are variable and many are not applicable to *in vivo* measurements. In this work, the water exchange kinetics of two prototype paramagnetic agents (PARACEST) are compared by using data from classic NMR linewidth measurements, by fitting CEST spectra to the Bloch equations modified for chemical exchange and by a method where CEST intensity is measured as a function of applied B_1. A relationship is derived that provides the water exchange rate from the X-intercept of a plot of steady-state CEST intensity *versus* $1/\omega_1^2$, referred to here as an Omega plot. Furthermore, it is shown that this relationship is independent of agent concentration. Exchange rates derived from Omega plots using either high resolution CEST NMR data or CEST data obtained by imaging agree favorably with exchange rates measured by the more commonly used Bloch fitting and linewidth methods. Thus, this new method potentially allows access to a direct measure of exchange rates *in vivo* where the agent concentration is typically unknown.

Introduction

A new class of MR imaging contrast agents called CEST and PARACEST agents (paramagnetic CEST) are characterized by water or proton exchange sites that differ from bulk water in their chemical shifts and are in slow-to-intermediate chemical exchange with bulk water molecules or protons (1). Selective RF irradiation of those unique water or proton sites can result in a reduction in total water magnetization, thereby providing a unique mechanism to introduce MR contrast into an image by RF frequency selection. Potential CEST sites include the many endogenous biopolymers containing exchangeable –NH and –OH protons (2) or exogenous diamagnetic (1) and paramagnetic agents with either exchangeable proton sites or, in the case of paramagnetic complexes, an exchanging water molecule (3,4). Numerous examples of paramagnetic CEST(PARACEST) agents have been reported including agents that respond to temperature (5,6), redox (7), pH (8), glucose (9), nitric oxide (10) and enzyme activity (11).

Address correspondence to ADS at the Advanced Imaging Research Center, University of Texas Southwestern Medical Center, 5323 Harry Hines Blvd., Dallas, TX 75390, dean.sherry@utsouthwestern.edu, Phone: 214-645-2730.

The PARACEST mechanism offers three advantages over paramagnetic Gd^{3+}-based complexes, superparamagnetic iron oxide particles and other relaxation agents for MR contrast. First, one can turn the CEST or PARACEST contrast on or off at will so it is easy to compare an experiment to a control just by shifting the irradiation away from the exchanging resonance(s). With relaxation agents, one compares pre-to post-injection images and hopes the subject does not move between images. Second, two PARACEST agents, targeted to two different biomarkers and having two different resonant frequencies, could be injected and selectively imaged, unambiguously, during the same exam. Slow uptake and slower washout of targeted agents make this less practical with relaxation agents. Without the saturating RF pulses, most PARACEST agents shorten T_2 but have little to no effect on T_1. This means that a relaxation agent could be used after a PARACEST exam without waiting. Finally, most CEST agents (endogenous and exogenous) are inherently pH sensitive and it is relatively easy to design PARACEST agents that respond to the presence of other metabolites (glucose) or other biological indices. These allow easy pH mapping in phantoms where the agent concentration is known but require corrections for concentration differences in vivo. Approaches to solve this problem include a second “unresponsive” agent to act as a concentration marker (12) and CEST agents with two different chemical exchange sites, one responsive and one unresponsive (8,13). In the latter case, the two sites are activated separately by selective irradiation and the ratio of the two effects is independent of concentration (13). An additional option we consider here is to measure the dependent parameter, the proton chemical exchange lifetime in the case of a pH sensor, directly. The proton chemical exchange lifetime is a fundamental feature of the agent chemistry and in principle should be independent of concentration.

Despite these stated advantages, the practical use of PARACEST agents has yet to be fully realized largely because they do require RF activation and this is not as easily done *in vivo* as *in vitro*. Most tissues have an inherent background signal after RF activation due to transfer of spin magnetization from the tissue lattice to bulk water, the so called MT effect (14). MT contrast can be substantial in tissues and can obscure contrast due solely to a CEST or PARACEST agent so this must be taken into account before PARACEST agents can reach their full potential.

There are several existing NMR methods that can be used to measure proton or water exchange rates in such complexes, classic temperature-dependent linewidth measurements, fitting of CEST spectra to the Bloch equations modified for NMR exchange (15), and the WEX, QUEST and QUESP methods summarized by McMahan et al. (16). Each of these methods requires that the agent concentration be known. In search of a method to measure exchange rates and concentrations in vivo, we introduce here a modified version of QUESP that allows an estimate of both τ_M and the agent concentration. Here, the theory behind this new method is presented and water exchange rates determined by classical linewidth *versus* temperature measurements, fitting of CEST spectra collected at a single temperature, and the new method are compared for two model PARACEST agents, the widely-studied EuDOTA-$(gly)_4^-$ anion and the ester of this same complex, EuDOTA-$(gly\text{-}OEt)_4^{3+}$. The chemical structures of these two model PARACEST agents are shown in Figure 1.

Theory

For any pool of NMR spins undergoing continuous RF saturation “on-resonance”, the NMR signal intensity at steady-state is described by (15),

$$Mz^{ss} = \frac{Mz^{o}}{1+\omega_1^2/(R_1 R_2)} \quad [1]$$

where M_z^o is the equilibrium magnetization in the absence of RF saturation, ω_1 is the B_1 magnetic field strength of the saturation RF pulse in radians/s, and R_1 and R_2 are the longitudinal and transverse relaxation rates of the spin pool, respectively. If this pool is also exchanging spins with another pool during this process, then an exchange term can be added to each relaxation rate as follows,

$$Mz^{ss} = \frac{Mz^{o}}{1+\omega_1^2/((R_1+k)(R_2+k))} \quad [2]$$

where k is the rate at which these spins leave this pool and enter the other pool. Assuming that this rate is fast relative to the relaxation rates, i.e., $k \gg R_1$ and $k \gg R_2$ (experimental evidence to support this assumption is given under Results), equation 2 simplifies to,

$$\mathrm{m} = \frac{1}{1+\omega_1^2/k^2} \quad [3]$$

For simplicity, M_z^{ss}/M_z^o is temporarily given the symbol m. This equation holds for any pool of spins undergoing continuous RF saturation. To describe specific pools, we define m^a as the bulk water pool and, for the particular case of a Eu^{3+}-based PARACEST agent, m^b as the Eu^{3+}-bound water pool.

Now, if one saturates the Eu^{3+}-bound water pool using a frequency selective RF pulse (ω_1), then these saturated or partially saturated spins will move into the bulk water pool at a rate, k^b, resulting in loss of magnetization in the bulk water signal. If the Eu^{3+}-bound water is fully saturated, m^b would by definition be zero. If partially saturated, $0 < m^b < 1$. The rate of loss of magnetization in the bulk water pool due to exchange depends upon both k_b and the fractional saturation in the Eu^{3+}-bound water pool, $1 - m^b$. So, if one defines the product, $(1 - m^b)\, k_b$ as R_{CEST}, equation 4 follows from equation 3.

$$R_{CEST} = (1 - m^b)\, k_b = \frac{{\omega_1}^2/k_b}{1+\omega_1^2/{k_b}^2} \quad [4]$$

After a prolonged period of RF saturation on the Eu^{3+}-bound water resonance and the system has reached steady state, the magnetization remaining in the bulk water pool is determined by R_{CEST} and the rate of recovery of bulk water magnetization due to T_1. In the equations that follow, we use the term c/55.5 as the fraction of protons in the bound pool (the agent) relative to the total water. This term strictly applies to aqueous samples only (in vitro samples). For the more general case (i.e., tissue), c/55.5 should be replaced with $(n)c_{agent}/c_{water}$ where n is the number of exchangeable protons on the agent, c_{agent} is the concentration of the agent in the tissue, and c_{water} is the concentration of water protons in the tissue. The value of c_{water} can be estimated independently using a proton density weighted imaging sequence. Hence, for in vitro conditions,

$$(1 - m^a)R_1{}^a = \frac{c}{55.5} m^a R_{CEST} \quad [5]$$

By combining equations 4 and 5, one arrives at,

$$\frac{m^a}{1 - m^a} = \frac{55.5}{c} k_b R_1{}^a \left(\frac{1}{k_b{}^2} + \frac{1}{\omega_1{}^2} \right) \quad [6]$$

Since CEST spectra are presented as plots as M_z^{ss}/M_o, it is useful to convert equation 6 into,

$$\frac{M_z^{ss}}{M_o - M_z^{ss}} = \frac{55.5}{c} k_b R_1{}^a \left(\frac{1}{k_b{}^2} + \frac{1}{\omega_1{}^2} \right) \quad [7]$$

Thus, a plot of $M_z^{ss}/(M_o - M_z^{ss})$ versus $1/\omega_1{}^2$ should be linear with a slope of $55.5R_1{}^a k_b/c$ and a Y-axis intercept of $55.5R_1{}^a/(k_b{}^* c)$ while the X-axis intercept (when $M_z^{ss}/(M_o - M_z^{ss}) = 0$) provides a direct readout of the exchange rate, $-1/k_b{}^2$. The power of this method is that k_b can be determined without knowing concentration or relaxation rate. The determination of the agent concentration in tissue requires knowledge of the value of $R_1{}^a$. Since the concentration of agent in tissue will be low and the relaxivities of these agents are also low, one can use the intrinsic value for R_1 of the tissue as an estimate for $R_1{}^a$. Given this assumption and the k_b as determined from the intercept, then the concentration, c, can be derived from the slope. Equation [7] can also be derived from the Bloch-McConnell equations using identical assumptions.

This analysis assumed that measurements of magnetization were performed at steady state following a very long saturating pulse. It is straightforward to show that the same analysis applies to magnetization measurements obtained using the imaging sequence shown in Figure 2, which uses saturation pulses applied for durations that are much shorter than T_1. In this approach, CEST pulses alternate with observation pulses and acquisitions and these pulse trains repeat at intervals of TR/N, where N is the number of slices imaged. In this case, the longitudinal magnetization varies as a result of relaxation processes, observation pulses, and the application of CEST pulses. In this imaging sequence, the signal-to-noise and contrast are determined primarily by the central k-space lines and thus it is the magnetization at this point in the data collection that determines the CEST effect. If linear k-space sampling is employed for a 128×128 acquisition, the steady state condition will occur after 64 TR intervals. If we employ a 100 ms TR with a 50 ms Fermi pulse for CEST saturation (50% duty cycle), steady state is reached after 6.4 sec with 3.2 sec of CEST saturation. These parameters are similar to those used when the CW saturation employed. Note that if a large number of slices are chosen, TR can become longer than T_1 and steady state is then virtually identical to that following a long saturation pulse. Taking all of these considerations into account, we can derive the same expression as is shown in equation 7 for CEST imaging sequence shown in Figure 2.

An implicit assumption of this straight line analysis is that the bound to free pool chemical shift difference, which was not considered at all, is much larger than ω_1. This condition keeps the free water magnetization pointing along the z axis. If ω_1 is increased to violate this condition, the plot curves upward. Going the other way, decreasing ω_1, the plot becomes too noisy; m approaches 1 and 1-m can be positive, negative, or zero. An anonymous reviewer

notes that when Eq. [7] is multiplied, term by term, by ω_1^2, the result plots as a straight line against ω_1^2, again with the x intercept determining k_b. For two point analyses, the two methods give the same k_b. With more than two points, the plot against ω_1^2 has more favorable noise propagation than the plot against $1/\omega_1^2$.

Materials and Methods

Chemistry

All solvents and reagents were purchased from commercial sources and used without purification unless otherwise stated. ^{1}H and ^{13}C NMR spectra were recorded on a Varian 400 spectrometer operating at 400 and 100 MHz, respectively. MALDI mass spectra were acquired using a Applied Biosystems Voyager-6115 mass spectrometer. The ligands 1,4,7,10-tetraazacyclododecane-1,4,7,10-tetrakis(ethyl-acetamidoacetate) (**1**) and 1,4,7,10-tetraazacyclododecane-1,4,7,10-tetrakis(acetamidoacetate) (**2**) and their europium complexes were synthesized according to literature procedures (17,18).

CEST spectra

All CEST spectra were recorded using a 400 MHz Varian INOVA spectrometer and a 5 mm NMR tube and a D_2O capillary insert for locking. CEST spectra were obtained by applying a selective pre-saturation pulse for an indicated period of time at regular intervals of frequency, arrayed between ± 40,000 Hz and in steps of 200 Hz. The repetition time (d1) between scans was 10 s and acquisition time 1 s. The plot of saturation frequency versus the water signal intensity results in a CEST spectrum. Variable temperature NMR measurements were done using the Varian VT controller and either nitrogen or air for purging. The system was calibrated using a methanol standard. Low temperature measurements were collected by purging dry nitrogen gas through a liquid nitrogen bath prior and the controller to warm the N_2 back to the desired temperature.

Fitting the CEST spectra to the Bloch equations modified for exchange

The water exchange rates were calculated by fitting the experimental CEST spectra to a three pool (bound water and amide protons exchanging with bulk water) model based on the numerical solutions obtained from modified Bloch equations (15) written in MATLAB (The Mathworks Inc., Natick, MA). The applied power (B_1) in Hz, the presaturation time, concentrations of exchanging bound water protons and amide protons, T_1 (bulk water), T_2 (bulk water), and chemical shifts of the Eu^{3+}-bound water exchange peak and the complex –NH protons were included as known parameters. Initial estimates of τ_M (bound water lifetime) were given along with an upper and lower boundary values, typically 10–500 μs. B_1 values were calibrated prior to collection of the CEST spectra by measuring the 360° pulse width for bulk water protons as a function of transmitter power level.

Omega plots

Omega plots ($M_z/(M_o - M_z)$ *vs* $1/\omega_1^2$ (ω_1 in rad/sec)) were derived from measures of the bulk water signal intensity at steady state (M_z^{ss}) after a 10 s presaturation pulse on the Eu^{3+}-bound water exchange peak using a series of applied B_1 values. The X-axis intercept ($-1/k_b^2$) gives the rate at which water leaves the Eu^{3+}-bound water site. These were used to derive theEu^{3+}-bound water lifetime (τ_M).

Water exchange rates from temperature dependent linewidth data

The “gold standard” for slow-to-intermediate exchanging systems is to measure NMR linewidths as a function of temperature. The bound water resonance and the bulk water resonance near 0 ppm were fitted to a classical 2-site exchange model using an exchange

fitting routine in the NMR software package, ACD (Advanced Chemistry Development, Inc., Toronto).

Imaging

Images were collected using in a transmit receive coil 18 cm long with 10 cm diameter in a 1.5 T Signa scanner (GE Healthcare, Waukesha, WI). The phantom data of Fig 6 came from 70 mm long Eppendorf centrifuge tubes, tapered over about a third of their length. One contained only water, one 20 mM, and one 60 mM EuDOTA-$(gly)_4^-$. This agent has a chemical shift of 52 ppm or 3320 Hz at 1.5 T. Slices were 8 mm thick separated by 10 mm gaps. FOV was 12×12 cm with a 128×128 matrix, the observe flip angle was 18° and TE = 6 ms. Three interleaved slices were imaged with TR of 300 (100 ms per slice). With 2 averages per scan, total scan time was 2 × 128 × 0.3s = 77s. Phase encoding steps went from most negative to most positive, assuring that steady state was reached long before sampling the center of k-space. The saturation pulses for CEST were Fermi shaped each having 50 ms duration, one before each observation pulse, as illustrated in Figure 2. For control experiment at 1.5 T, the saturation pulse frequency offset from bulk water resonance was reversed.

Results

Eu^{3+}-bound water linewidths as a function of temperature

The “gold standard” NMR method for measuring exchange rates in slow-to-intermediate exchanging systems is to monitor NMR linewidths of two exchanging pools as a function of temperature. Of the two agents examined here, only the ester, EuDOTA-$(gly\text{-}OEt)_4^{3+}$, is amenable to such measurements in water because this is the only complex of the two that the water exchange is slow enough to allow direct observation of the Eu^{3+}-bound water resonance over a wide temperature range, from about 4–42°C. The bound water molecule in EuDOTA-$(gly)_4^-$ can be detected at low temperatures in mixed aqueous solvents but it is difficult to detect in pure water as solvent. The results of a temperature dependent study of the Eu^{3+}-bound water resonance in EuDOTA-$(gly\text{-}OEt)_4^{3+}$ over the temperature range 4–38°C shown in Figure 3. In addition to the linewidth changes observed here, the bound water resonance shifts from ~57 ppm at 4°C to ~38 ppm at 38°C due to the hyperfine shift effects of the paramagnetic Eu^{3+} ion. The bound and bulk water resonances were fit to a classical 2-site exchange model using the linewidth fitting routine in the NMR software package, ACD (Advanced Chemistry Development, Inc., Toronto). This resulted in the exchange lifetimes reported next to each calculated spectrum in Figure 3. Interesting, the bound water lifetime changes about 1 order of magnitude over this limited temperature range. The Arrhenius plot of these data gave an activation energy of 13 kcal/mol for water exchange in this system.

CEST spectra of this same complex were also collected as a function of temperature using a singleB_1 (162 Hz) and at a single controlled temperature (25°C). The CEST spectra of Figure 4a also change dramatically with temperature as expected. However, unlike the linewidth data of Fig. 3, these spectra show that water exchange is somewhat too slow for optimal CEST at 4°C, is about optimal by 15°C (maximum CEST intensity at this temperature and applied power), and somewhat too fast for optimal CEST at the higher temperatures. The CEST exchange peak also shifts upfield toward the bulk water resonance with increasing temperature as expected for a hyperfine shifted resonance in a paramagnetic complex such as this. A fit of these individual CEST spectra to the Bloch equations for 3-site exchange (Eu^{3+}-bound water, the four –NH protons, and bulk water) gave τ_M values of 896 μs, 880μs, 641μs, 210±6 μs, and 93±2 μs for the 4°C, 10°C, 15°C, 25°C and 37°C, respectively. These values are, on average, within 9% of the lifetimes determined by direct NMR linewidth fitting (Fig. 3).

Omega plots for determining exchange rates

The derivation of the linear relation shown as equation 7 requires the assumption $k_b \gg R_1$ and R_2 or, equivalently, $\tau_M \ll T_1$ and T_2 of the bound water protons in these EuDOTA-tetraamide complexes. There are various approaches to test these boundary conditions. Luz and Meiboom (19) have shown that the T_1 of bulk water in the presence of paramagnetic ions obeys the following relationship,

$$\frac{1}{T_{1P}} = \frac{p_M}{(T_{1M} + \tau_M)} \quad [8]$$

where p_M is the fraction of exchangeable protons in the PARACEST agent, T_{1M} is the T_1 of the inner-sphere water molecule and τ_M is the lifetime of the bound water molecule in the chelate. For 20 mM and 60 mM solutions of EuDOTA-$(gly)_4^-$ the bulk water T_1's measured at 25°C were 2.9 s and 2.62 s, respectively. A plot of $1/T_1$ *versus* p_M for these two data points yields a slope of 50.875 which gives an estimate for $(T_{1M} + \tau_M)$ of 19.6 ms. Given that τ_M for this complex as measured either by the linewidth method (210±6 μs) or CEST fitting (225 μs) are no more than 1% of the sum of $(T_{1M} + \tau_M)$ and $T_{1M} = T_{2M}$ for paramagnetic systems such as these, clearly the assumptions needed to simplify equation 2 to equation 3, $k_b \gg R_1{}^b$ and $k_b \gg R_2{}^b$, are easily met. For other lanthanide complexes such as Tm^{3+} or Yb^{3+}-based systems, the same restrictions apply. Water exchange in these later complexes tends to be considerably faster than in Eu^{3+}-based systems (20) so the condition, $k_b \gg R_1$ and R_2, should be even easier to meet than with the Eu^{3+} complexes used here. Nevertheless, the R_1 and R_2 are also faster with these other ions (especially Tm^{3+}-based systems) so it will be important to demonstrate that this condition is met for each potential PARACEST agent.

Plots of $M_z^{ss}/(M_o - M_z^{ss})$ versus $(1/\omega_1{}^2)$ (equation 7, henceforth referred to as Omega plots) for three different samples of EuDOTA-(gly-OEt)$_4{}^{3+}$ (5, 10 and 20 mM) collected at 25°Care shown in Figure 4. The X-axis intercepts of these three plots provide a third independent measure of $1/k_b$ or, equivalently, τ_M. The intercepts gave an average value for $\tau_M = 247 \pm 24$ μs, similar to the values obtained by the other two methods at this same temperature. Furthermore, the relative slopes of these plots were in the ratio, 4:2:1, exactly as predicted by equation 7. These combined data demonstrate that equivalent exchange rates can be determined by temperature dependent linewidth measurements, CEST fitting, and the Omega plot method described herein.

The hydrolyzed form of this same compound, EuDOTA-$(gly)_4^-$ is known to display somewhat faster water exchange than the parent ester compound. This complex, unlike the ester analog, has been shown to be quite tolerant in small animals *in vivo* (21) so it was of interest to determine whether identical bound water lifetimes could be obtained by fitting the CEST spectra of this complex *versus* the Omega plots. Figure 5 shows CEST spectra of 20 mM EuDOTA-$(gly)_4^-$ collected at different B_1 values plus an Omega plot collected using spectroscopic methods (10 s presaturation pulse). A fitting of CEST spectra to a 3-pool exchange model gave a τ_M value of 160 ± 30 μs. The X-axis intercept of the Omega plot of Figure 5 gave an identical τ_M value of 156± 10 μs. This verifies that the method also works for agents with faster water exchange than the ester described earlier.

Omega plots were also collected on two different concentrations of EuDOTA-$(gly)_4^-$ using a 1.5 T clinical imaging scanner and using a train of 50 ms pulses each interleaved with a k-space data sampling, as compared to using a single long pulse of 10 s duration followed by a z-magnetization readout pulse in spectroscopic CEST method. The resulting plots were

linear (Figure 6) and the X-axis intercept gave τ_M values of 227 and 222 μs for the 20 mM and 60 mM samples, respectively. The relative slopes of these plots were 3:1. Given the observation that the temperature was not strictly controlled in the later experiment and the ambient temperature of the imaging room was approximately 20–22°C, a longer lifetime was indeed expected based upon the temperature dependent data shown for the ester derivative. The τ_M value expected for this sample at 25°C was 160 ± 30 μs but based upon the assumption that the activation energies for the two PARACEST agents examined here are similar, one would anticipate that a lifetime of about 220 μs for a temperature of 20–22°C (see Figure 3).

Discussion

The application of CEST methods to image biological processes *in vivo* is attractive because the technique is based on one of the most fundamental properties of biology, chemical exchange. This makes the measurement chemical exchange rates *in vivo* of paramount importance, especially for exogenous agents designed to respond to biological processes. In this report, we compared water exchange rates in two different Eu^{3+}-based PARACEST agents, a positively charged complex, EuDOTA-(gly-OEt)$_4^{3+}$ and the hydrolyzed anionic complex, EuDOTA-(gly)$_4^-$. Although the positively charged complex may not be suitable for use *in vivo* for toxicity reasons, it was chosen for study here because the Eu^{3+}-bound water molecule in this complex exchanges slowly enough with solvent water to actually detect the bound water peak by high resolution NMR even at near 40°C (17). This allowed a direct comparison of water exchange rates as measured by using three methods, the “gold standard” temperature-dependent linewidth method, fitting of CEST spectra to the Bloch equations, and the Omega plots described herein. The bound water lifetimes in this complex determined by the three methods gave values of 225±10 μs, 210±6 μs and 247±24 μs, respectively. The temperature-dependent linewidth data were useful because they provided a clear visual picture of exactly how sensitive water exchange is to temperature in these complexes, changing 10-fold over the range, 4–38°C. The fact that the bound water lifetime decreased by just over a factor of two between 25 and 38°C also illustrates how important it is to keep this fact in mind when designing agents for use at physiological temperatures.

The hydrolyzed, anionic form of this same complex, EuDOTA-(gly)$_4^-$, has been shown to quite safe for use in small animals (21). Although considerably less stable thermodynamically than the analogous carboxylate complex, EuDOTA$^-$, the release of free metal ion from EuDOTA-(gly)$_4^-$ (dissociation kinetics) is so slow in comparison to the more common carboxylate complexes that the acute toxicity is also extraordinarily low. Both complexes, the carboxylate and the tetraamide, distribute equivalently into all extracellular space *in vivo* and are cleared quickly as intact complexes exclusively by renal filtration (21). These data suggest that EuDOTA-(gly)$_4^-$ should be a good candidate for use as a PARACEST agent in small animals. However, the question of whether this complex has an optimal water exchange rate at 37°C remained unanswered. We recently demonstrated that a Eu^{3+}-based PARACEST agent with water exchange characteristics similar to that of EuDOTA-(gly)$_4^-$ can be detected by CEST imaging in mice but that interference from tissue magnetization transfer effects are problematical (Todd Soesbe, personal communication). The agent used in that study (EuDOTA-(Me$_2$gly)$_4^-$) has an even shorter bound water lifetime (28 μs) than EuDOTA-(gly)$_4^-$ (52 ± 3 μs) at 37°Cso the fact that EuDOTA-(Me$_2$gly)$_4^-$ could be detected at all indicates that an agent with an optimal water exchange lifetime at body temperature should be readily detected even in the presence of tissue MT effects. Given the known relationship between applied power in the PARACEST experiment and the optimal exchange rate for the agent (optimal rate = $2\pi B_1$ (15)), one can predict that an agent with a bound water lifetime of 1.6 ms would work best for an applied B_1 field of 100 Hz or 0.8 ms for 200 Hz, etc. at 37°C. This means that new PARACEST

agents will need to be discovered that exchange water 10–30 times slower than current agents at 37°C.

McMahon et al. (16) recently described two methods for determining exchange rates from CEST data, QUEST (Quantifying Exchange rates in Saturation Transfer Agents Using Saturation Time) and QUESP (Quantifying Exchange rates in Saturation Transfer Agents Using Saturation Power). One of these methods, QUESP, derived from the Bloch equations modified for exchange, is similar to the Omega-plot method described herein. In QUESP, the exchange rates are determined by fitting the changes in the water signal intensities after application of different saturation powers to an equation containing a number of parameters including the concentration of CEST agent (see Figures 6A and B in (16)). The approach presented here is an extension of QUESP with the major advantage that the Omega plots give the exchange rates independent of the concentration of the agent present in solution. Practically, constructing Omega plots will require the acquisition of PARACEST data using at least two B1 values and one additional off-resonant control irradiation (although collection and fitting of a complete CEST spectrum may be necessary whenever tissue MT effects dominate CEST from the agent (22)). If the water concentration may be assumed or measured and the relaxation rate is measured, a combination of the x-intercept, which is concentration independent, and the slope, which is not, the agent can be fully characterized *in vivo*. This approach can be applied most simply in cases where knowledge of the water exchange lifetime alone is desired. It may be applied with a supplementary relaxation measurement when the agent concentration or concentration and exchange rate is required in order to analyze the PARACEST effect of a responsive (or targeted) agent to derive a physiologically relevant parameters such as pH, temperature, or the presence of certain metabolites.

In summary, we have presented concentration independent approach to characterizing the effects of a PARACEST agent, referred to here as Omega plots. We have validated the Omega plot approach against more conventional NMR methods for measuring water exchange lifetimes and found excellent agreement *in vitro*. Moreover, our results demonstrate that the assumptions necessary to derive the Omega plots are valid for the class of the Eu-DOTA-tetramide chelates and derivatives thereof. We have also found that the rates of water exchange are very sensitive to temperature in the range of 20–38°C. This behavior should be considered when designing and characterizing Eu-DOTA based PARACEST agents for use in vivo.

Acknowledgments

The authors acknowledge financial support from the National Institutes of Health (CA-115531, CA-126608, RR-02584 and EB-004582) and the Robert A. Welch Foundation (AT-584).

References

1. Ward KM, Aletras AH, Balaban RS. A New Class of Contrast Agents for MRI Based on Proton Chemical Exchange Dependent Saturation Transfer (CEST). Journal of Magnetic Resonance 2000;143(1):79–87. [PubMed: 10698648]
2. Zhou JY, Lal B, Wilson DA, Laterra J, van Zijl PCM. Amide proton transfer (APT) contrast for imaging of brain tumors. Magnetic Resonance in Medicine 2003;50(6):1120–1126. [PubMed: 14648559]
3. Zhang S, Merritt M, Woessner DE, Lenkinski RE, Sherry AD. PARACEST Agents: Modulating MRI Contrast via Water Proton Exchange. Accounts of Chemical Research 2003;36(10):783–790. [PubMed: 14567712]
4. Zhang S, Winter P, Wu K, Sherry AD. A Novel Europium(III)-Based MRI Contrast Agent. Journal of the American Chemical Society 2001;123(7):1517–1518. [PubMed: 11456734]

5. Zhang S, Malloy CR, Sherry AD. MRI Thermometry Based on PARACEST Agents. Journal of the American Chemical Society 2005;127(50):17572–17573. [PubMed: 16351064]
6. Li AX, Wojciechowski F, Suchy W, Jones CK, Hudson RHE, Menon RS, Bartha R. A sensitive PARACEST contrast agent for temperature MRI: Eu^{3+}-DOTAM-glycine (Gly)-phenylalanine (Phe). Magnetic Resonance in Medicine 2008;59(2):374–381. [PubMed: 18228602]
7. Ratnakar SJ, Woods M, Lubag AJM, Kovacs Z, Sherry AD. Modulation of Water Exchange in Europium(III) DOTA-Tetraamide Complexes via Electronic Substituent Effects. Journal of the American Chemical Society 2008;130(1):6–7. [PubMed: 18067296]
8. Aime S, Castelli DD, Terreno E. Novel pH-reporter MRI contrast agents. Angew Chem Int Ed 2002;41(22):4334–4336.
9. Zhang S, Trokowski R, Sherry AD. A Paramagnetic CEST Agent for Imaging Glucose by MRI. Journal of the American Chemical Society 2003;125(50):15288–15289. [PubMed: 14664562]
10. Liu G, Li Y, Pagel MD. Design and characterization of a new irreversible responsive PARACEST MRI contrast agent that detects nitric oxide. Magnetic Resonance in Medicine 2007;58(6):1249–1256. [PubMed: 18046705]
11. Yoo B, Raam MS, Rosenblum RM, Pagel MD. Enzyme-responsive PARACEST MRI contrast agents: a new biomedical imaging approach for studies of the proteasome. Contrast Media & Molecular Imaging 2007;2(4):189–198. [PubMed: 17712869]
12. Raghunand N, Howison C, Sherry AD, Zhang S, Gillies RJ. Renal and systemic pH imaging by contrast-enhanced MRI. Magnetic Resonance in Medicine 2003;49(2):249–257. [PubMed: 12541244]
13. Pikkemaat JA, Wegh RT, Lamerichs R, van de Molengraaf RA, Langereis S, Burdinski D, Raymond AYF, Janssen HM, de Waal BFM, Willard NP, Meijer EW, Grüll H. Dendritic PARACEST contrast agents for magnetic resonance imaging. Contrast Media & Molecular Imaging 2007;2(5):229–239. [PubMed: 17937448]
14. Wolff SD, Balaban RS. Magnetization transfer contrast (MTC) and tissue water proton relaxation *in vivo*. Magnetic Resonance in Medicine 1989;10(1):135–144. [PubMed: 2547135]
15. Woessner DE, Zhang S, Merritt ME, Sherry AD. Numerical solution of the bloch equations provides insights into the optimum design of PARACEST agents for MRI. Magnetic Resonance in Medicine 2005;53(4):790–799. [PubMed: 15799055]
16. McMahon MT, Gilad AA, Zhou J, Sun PZ, Bulte JWM, van Zijl PCM. Quantifying exchange rates in chemical exchange saturation transfer agents using the saturation time and saturation power dependencies of the magnetization transfer effect on the magnetic resonance imaging signal (QUEST and QUESP): pH calibration for poly-L-lysine and a starburst dendrimer. Magnetic Resonance in Medicine 2006;55(4):836–847. [PubMed: 16506187]
17. Zhang S, Wu K, Biewer MC, Sherry AD. ^{1}H and ^{17}O NMR Detection of a Lanthanide-Bound Water Molecule at Ambient Temperatures in Pure Water as Solvent. Inorganic Chemistry 2001;40(17):4284–4290. [PubMed: 11487334]
18. Aime S, Barge A, Castelli EE, Fedeli F, Mortillaro A, Nielsen FU, Terreno E. Paramagnetic Lanthanide(III) complexes as pH-sensitive chemical exchange saturation transfer (CEST) contrast agents for MRI applications. Magnetic Resonance in Medicine 2002;47(4):639–648. [PubMed: 11948724]
19. Luz Z, Meiboom S. Proton relaxation in dilute solutions of Cobalt(2+) and Nickel(2+) ions in methanol and rate of methanol exchange of solvation sphere. Journal of Chemical Physics 1964;40(2686)
20. Zhang S, Wu K, Sherry AD. Unusually Sharp Dependence of Water Exchange Rate versus Lanthanide Ionic Radii for a Series of Tetraamide Complexes. Journal of the American Chemical Society 2002;124(16):4226–4227. [PubMed: 11960448]
21. Sherry AD, Caravan P, Lenkinski RE. A primer on gadolinium chemistry. Journal of Magnetic Resonance Imaging. 2009 in press.
22. Li AX, Hudson RHE, Barrett JW, Jones CK, Pasternak SH, Bartha R. Four-pool modeling of proton exchange processes in biological systems in the presence of MRI-paramagnetic chemical exchange saturation transfer (PARACEST) agents. Magnetic Resonance in Medicine 2008;60(5):1197–1206. [PubMed: 18958857]

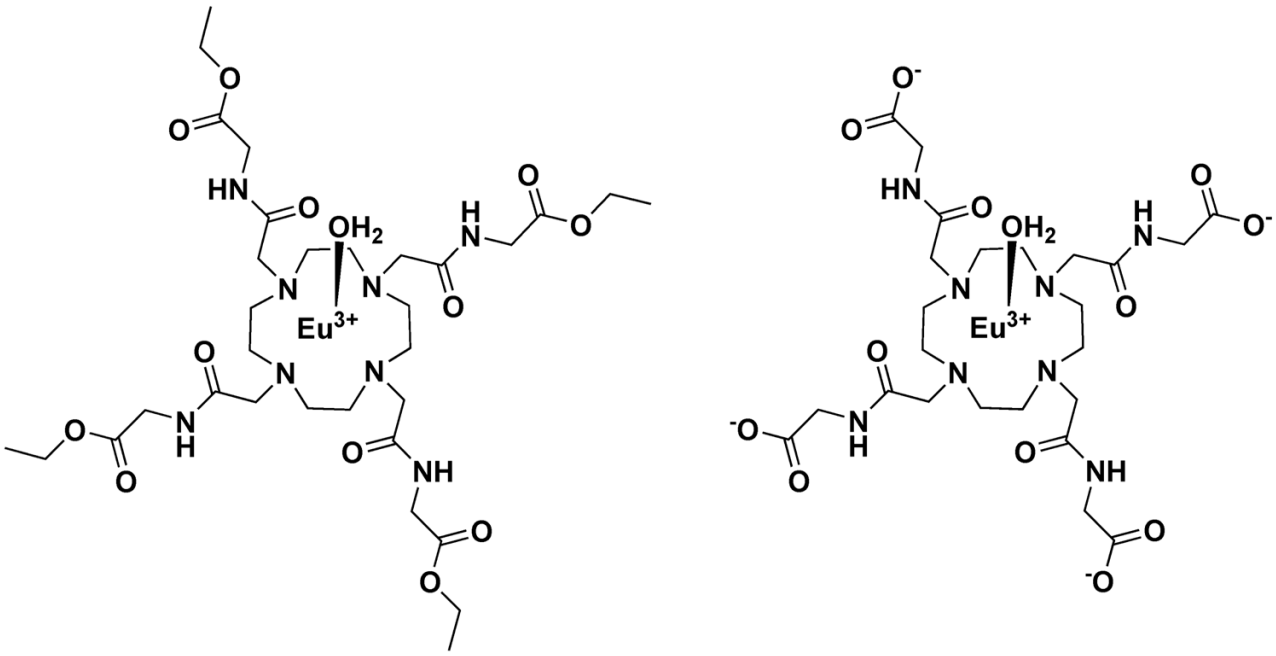

Figure 1.
Chemical structures of the two PARACEST agents examined in this study.

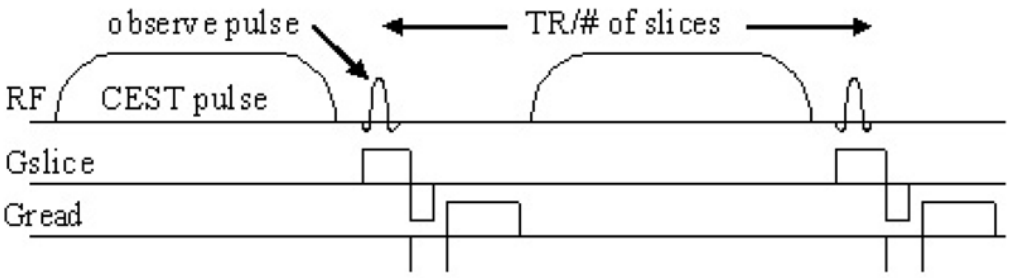

Figure 2.
Pulse sequence. The sequence is a standard 2D, multislice, gradient-echo sequence with a CEST saturation pulse inserted before each observation pulse.

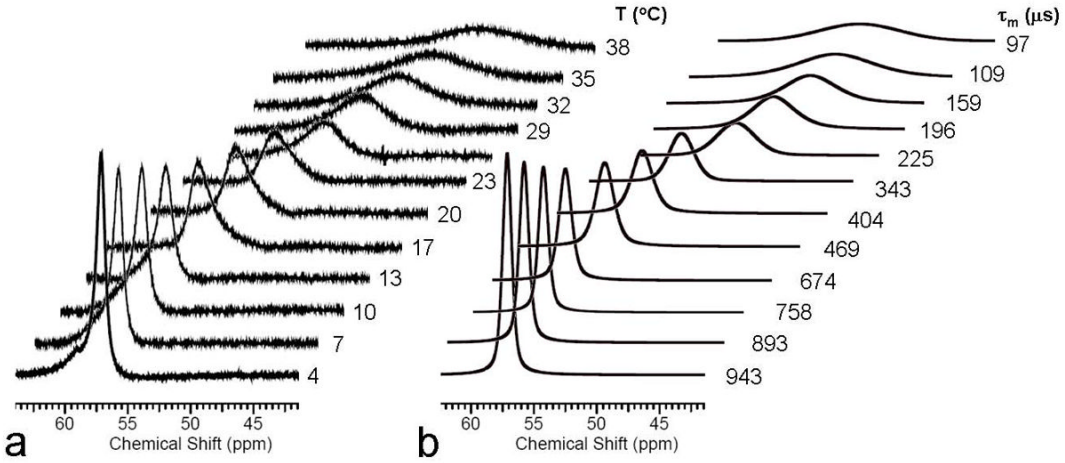

Figure 3.

a) High resolution ^{1}H NMR spectra of EuDOTA-(gly-OEt)$_4^{3+}$ in water at pH 7 (showing only the downfield region). The ^1H resonance near 57 ppm is the Eu^{3+}- bound water molecule. b) Calculated Eu^{3+}-bound water resonance at each temperature based upon line-fitting of the bound and bulk water resonances at each temperature. The bound water lifetimes at each temperature are shown.

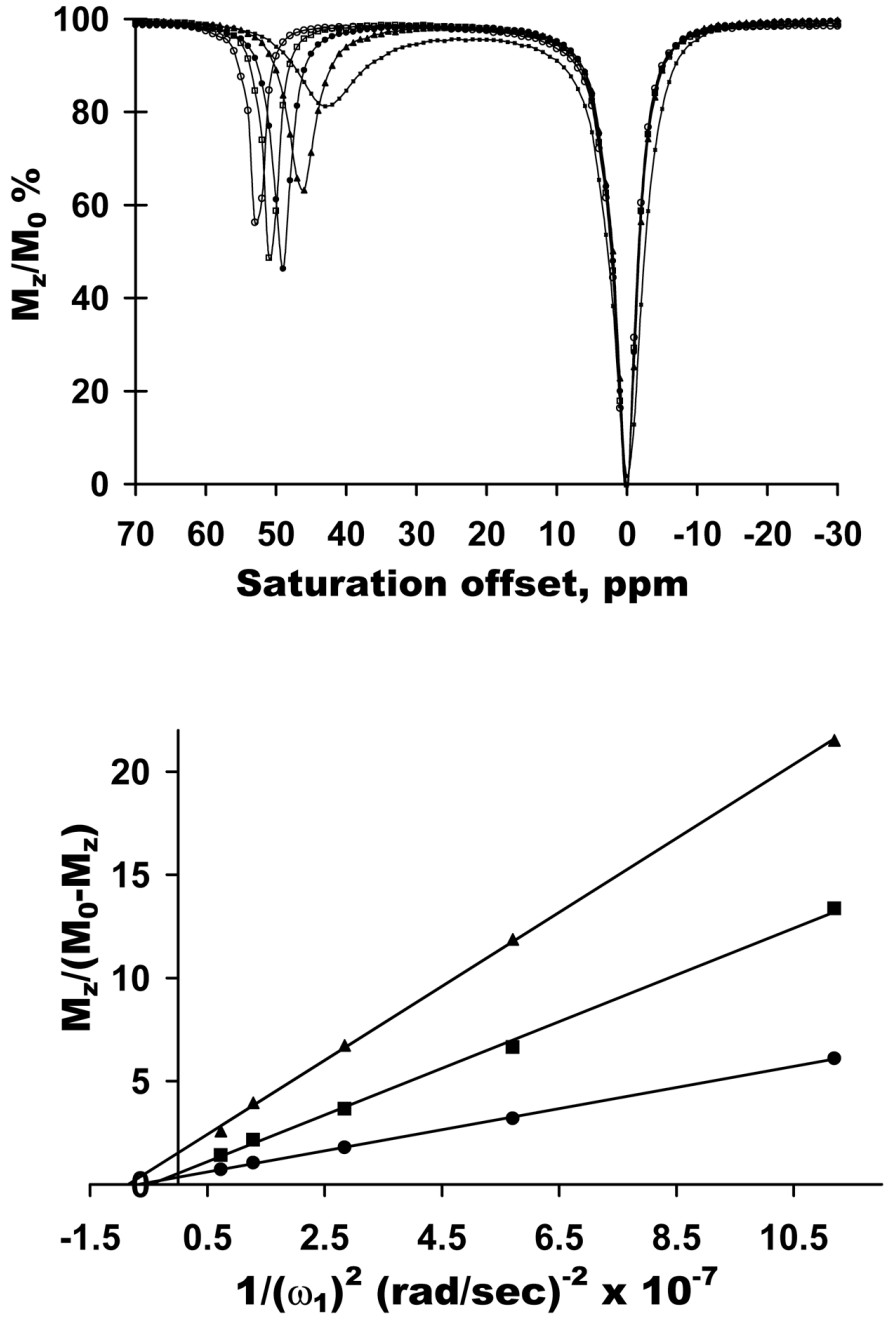

Figure 4.

a) CEST spectra of 20 mM EuDOTA(gly-OEt)$_4$ $^{3+}$ in water at pH 7, 9.4 T collected at temperatures of (■) 38ºC, (▲) 25ºC, (●) 15ºC, (□) 10ºC, and (○) 4ºC using a fixed B_1 = 162 Hz and a presaturation time of 3 s. b) An Omega plot - M_z /(100 − M_z) vs 1/B_1^2 – for 5 mM (▲), 10 mM (■) and 20 mM (●) Eu(DOTA-(glyOEt)$_4$)$^{3+}$ in water at pH 7 at 25°C using a 10 s saturation pulse at the indicated power levels.

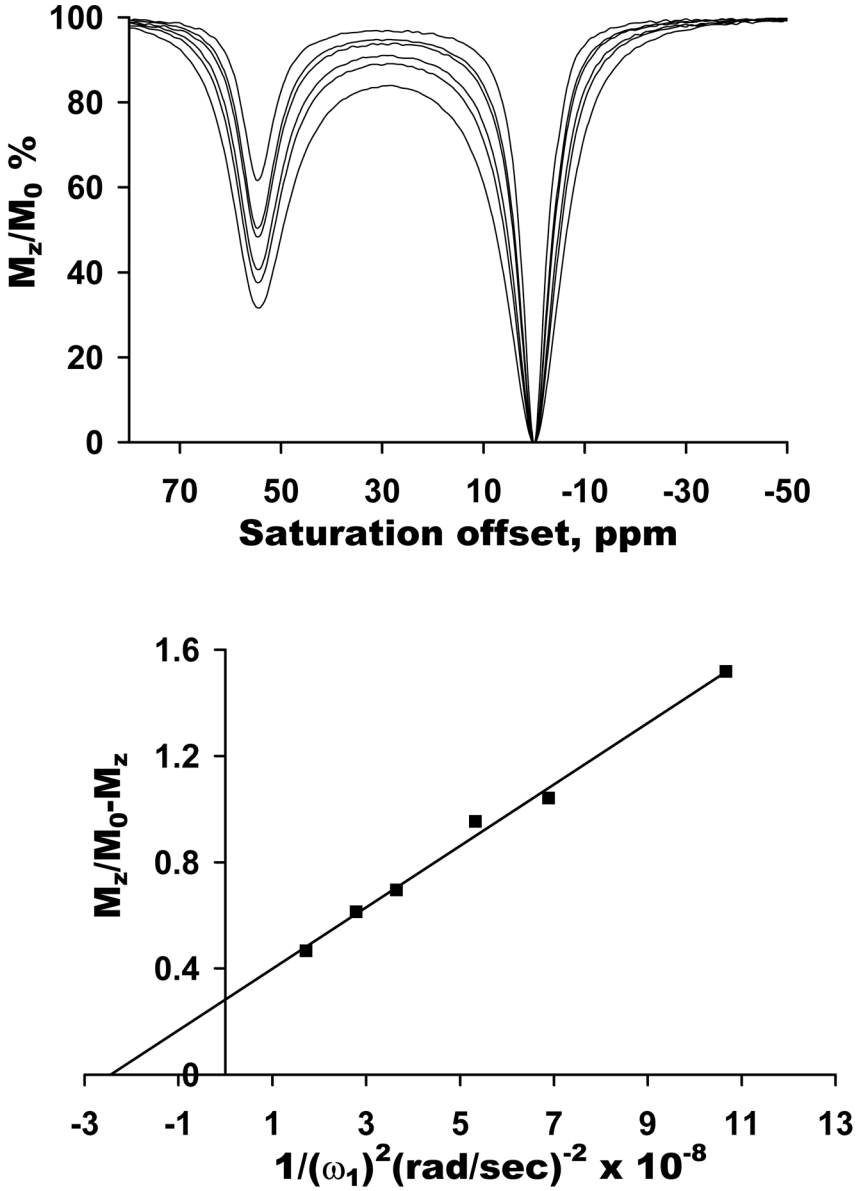

Figure 5.

a) CEST spectra of 20 mM EuDOTA(gly)$_4$ $^-$ in water at pH 7, 9.4 T collected 25ºC with varying B_1 = 487, 606, 689, 833, 952, 1212 Hz with a presaturation time of 10 s. b) An Omega plot − M_z /(100 − M_z) vs 1/B_1^2 for 20 mM Eu(DOTA-(gly)$_4$) $^-$ in water at pH 7 at 25°C using a 10 s saturation pulse at the indicated power levels.

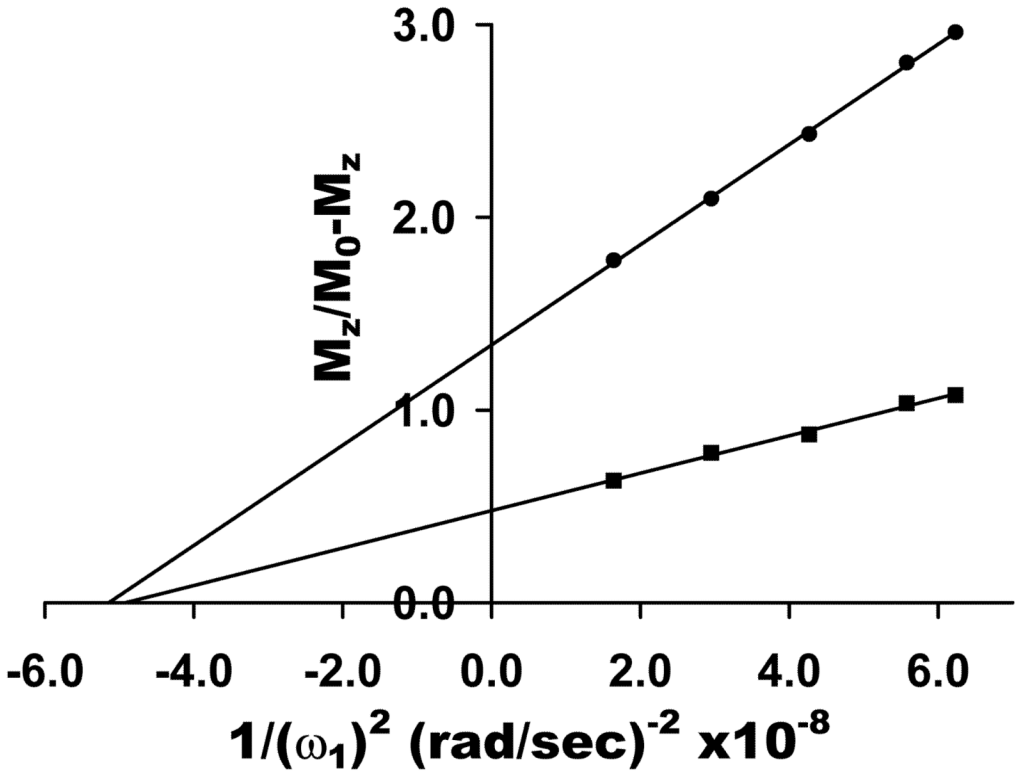

Figure 6.

An Omega plot derived from images collected using a 1.5T clinical scanner on phantom samples containing either 20 mM (●) or 60 mM (■) Eu (DOTA-$(gly)_4)^-$ dissolved in water at pH 7. The lines represent the linear least square fittings of the data.